Running head:

Integrated day-night model of leaf metabolism

Corresponding authors:

R.G. Ratcliffe and L.J. Sweetlove*
Department of Plant Sciences,
University of Oxford,
South Parks Road,
Oxford OX1 3RB
U.K.

+44 1865 275000
george.ratcliffe@plants.ox.ac.uk
lee.sweetlove@plants.ox.ac.uk

*For editorial correspondence and proofs

Journal area:

Systems and Synthetic Biology

A diel flux-balance model captures interactions between light and dark metabolism during day-night cycles in C_3 and CAM leaves.

C.Y. Maurice Cheung[1], Mark G. Poolman[2], David. A. Fell[2], R. George Ratcliffe[1] and Lee J. Sweetlove[1]

[1] Department of Plant Sciences, University of Oxford, South Parks Road, Oxford, OX1 3RB, UK
[2] School of Life Sciences, Oxford Brookes University, Headington, Oxford OX3 0BP, UK

One sentence summary:

A diel flux balance modeling framework that integrates temporally-separated metabolic networks provides realistic descriptions of light and dark metabolism in C_3 and CAM leaves, and suggests that energetics and nitrogen use efficiency are unlikely to have been drivers for the evolution of CAM.

Funding:

CYMC was supported by a studentship from the University of Oxford Systems Biology Doctoral Training Centre funded by the Clarendon Fund and a Sloane-Robinson award from Keble College, Oxford.

Corresponding authors:

R. George Ratcliffe, george.ratcliffe@plants.ox.ac.uk

* Lee J. Sweetlove, lee.sweetlove@plants.ox.ac.uk

* For editorial correspondence and proofs

ABSTRACT

Although leaves have to accommodate markedly different metabolic flux patterns in the light and the dark, models of leaf metabolism based on flux balance analysis (FBA) have so far been confined to consideration of the network under continuous light. A new FBA framework is presented that solves the two phases of the diel cycle as a single optimisation problem and thus provides a more representative model of leaf metabolism. The requirement to support continued export of sugar and amino acids from the leaf during the night, as well as to meet night-time cellular maintenance costs, forces the model to set aside stores of both carbon and nitrogen during the day. With only minimal constraints, the model successfully captures many of the known features of C_3 leaf metabolism, including the recently discovered role of citrate synthesis and accumulation in the night as a precursor for the provision of carbon skeletons for amino acid synthesis during the day. The diel FBA model can be applied to other temporal separations such as that which occurs in CAM photosynthesis, allowing a system-level analysis of the energetics of CAM. The diel

model predicts that there is no overall energetic advantage to CAM, despite the potential for suppression of photorespiration through CO_2 concentration. Moreover, any savings in enzyme machinery costs through suppression of photorespiration are likely to be offset by the higher flux demand of the CAM cycle. It is concluded that energetic or nitrogen-use considerations are unlikely to be evolutionary drivers for CAM photosynthesis.

INTRODUCTION

Photosynthetic metabolism continues to be studied intensively due to its importance for crop performance and for the global carbon cycle in relation to climate change. The metabolic pathways and enzymes involved in carbon fixation and related metabolic processes such as the synthesis of sucrose and starch have been well characterised. However, it is apparent that a full appreciation of leaf metabolism requires these metabolic processes to be placed in the context of the wider metabolic network (Szecowka et al., 2013). This is particularly important for predicting how strategies for engineering improved photosynthesis (Maurino and Weber, 2013) may affect network properties such as redox and energy balancing (Kramer and Evans, 2011).

Flux-balance analysis has emerged as the method of choice for predicting fluxes in large metabolic network models (Sweetlove and Ratcliffe, 2011) and several flux-balance models have explicitly considered photosynthetic metabolism in a variety of plants species and microorganisms. These include cyanobacteria (Knoop et al., 2010; Montagud et al., 2010; Nogales et al., 2012; Saha et al., 2012; Knoop et al., 2013), Chlamydomonas (Boyle and Morgan, 2009; de Oliveira Dal'Molin et al., 2011), Arabidopsis (de Oliveira Dal'Molin et al., 2010a), rapeseed embryos (Hay and Schwender, 2011), rice (Poolman et al., 2013), maize (Saha et al., 2011) and several C_4 plants (de Oliveira Dal'Molin et al., 2010b). These models successfully predicted the metabolic routes involved in the fixation of CO_2 into different biomass components in the light. However, one major feature of metabolism of photosynthetic organisms, namely the interactions between light and dark metabolism is neglected in most of these studies. Effectively, most models assume that the organism grows in constant light which is rarely true in natural conditions.

Apart from the obvious switch from photoautotrophic to heterotrophic metabolism between day and night, interactions between the two phases can occur through the temporal separation of storage compound synthesis and subsequent mobilisation. For example, it has been shown that the carbon skeletons used for nitrogen assimilation during the day are largely provided by carboxylic acids that were synthesised and stored during the previous night (Gauthier et al., 2010). Such temporal shifts of carbon and nitrogen metabolism have substantial implications for fluxes in the central metabolic network of leaves in the light (Tcherkez et al., 2009). Interactions between temporally separated metabolic events are also a critical

feature of crassulacean acid metabolism (CAM) photosynthesis in which CO_2 is initially fixed at night via PEP carboxylase, leading to night-storage of carboxylic acids (mainly malic acid) which are decarboxylated during the day to provide CO_2 for the conventional photosynthetic carbon assimilation cycle. While this is principally an adaptation to arid environments, there are unresolved questions as to whether CAM photosynthesis is energetically more efficient than C_3 photosynthesis (Winter and Smith, 1996). Such questions are becoming more important in the light of the proposed use of CAM plants as a source of biofuel (Yan et al., 2011).

One recent study has used flux-balance analysis to consider both light and dark metabolism in Synechocystis over a complete diel cycle divided into 192 time steps (Knoop et al., 2013). Time-courses of metabolic flux predictions over a diel cycle were simulated by altering the constraints on metabolic outputs (biomass composition) depending on the time-point and based on empirical rules. This led to a highly constrained model and did not allow the range of potential interactions between the day and night phases to be fully explored. We have developed an alternative modelling framework for integrated day-night flux-balance analysis in which the metabolic fluxes in the light phase and the dark phase were simulated simultaneously in a single optimisation problem. A pre-defined list of storage compounds that can accumulate freely over the diurnal cycle was made available to the model. The model was then free to choose amongst these storage compounds, the choice being dictated by the need to satisfy the objective function within the applied constraints. This diurnal modelling framework was used to explore the interactions between light and dark metabolism and to predict the metabolic fluxes in the light in both C_3 and CAM photosynthesis. We show that accounting for day-night interactions leads to an altered pattern of fluxes during the day that provides a better match with experimental observations. We were also able to simulate network flux distributions in CAM metabolism. The model successfully predicts the classical CAM cycle in the different CAM subtypes and allows a comparison of the energetic efficiency and metabolic costs between CAM and C_3 photosynthetic metabolism.

RESULTS

A day-night modelling framework for leaf metabolism

142 The aim was to construct a flux-balance model that accounted for the day and
143 night phases of leaf metabolism in an integrated fashion such that storage
144 compounds synthesised during the day were available for use in the dark and vice
145 versa. This was achieved by applying a specific framework of constraints to an
146 existing genome-scale model of Arabidopsis metabolism (Cheung et al., 2013). The
147 assumption was made that each phase (day and night) was in a pseudo-steady-
148 state, as has been done for previous flux-balance models of photosynthetic
149 metabolism. The two inter-dependent steady states were modelled as a single
150 optimisation problem with photoautotrophic metabolism specified in the day by
151 allowing a photon influx, and heterotrophic metabolism specified at night by setting
152 the photon influx to zero. For simplicity a 12 h-12 h day-night cycle was specified.
153 Also for simplicity, we considered the case of a mature leaf in which the only
154 metabolic outputs were the synthesis of sucrose and a range of amino acids for
155 export to the phloem. It is trivial to extend the model to consider a growing leaf and
156 to account for shorter or longer days.
157 The relative proportions of 18 amino acids exported to the phloem
158 (Supplemental Table 1) and the ratio of sucrose to total amino acid export (2.2:1)
159 were constrained in accordance with measurements of the composition of
160 Arabidopsis phloem exudate (Wilkinson and Douglas, 2003). The model was
161 required to maintain export of sugars and amino acids to the phloem during the day
162 and night, but at a ratio of 3:1 (day: night) based on measurements in Arabidopsis
163 rosettes (Gibon et al., 2004). The sole source of nitrogen for the leaf model was
164 nitrate import from the xylem, based on the observation that nitrate represents the
165 main form of nitrogen (80%) entering a leaf (Macduff and Bakken, 2003). The rate of
166 nitrate import into the leaf during the day and the night was constrained to be 3:2
167 based on measurements in various plant species (Delhon et al., 1995; Macduff and
168 Bakken, 2003; Siebrecht et al., 2003). Besides the export of sucrose and amino-
169 acids, cellular maintenance costs were accounted for by including generic ATPase
170 and NADPH oxidase steps for maintenance and the requirement to satisfy a
171 specified carbon conversion efficiency (Cheung et al., 2013). In this case, we
172 assumed a carbon conversion efficiency of 50% during the night based on the day-
173 night carbon balance calculated from measurements in Arabidopsis rosettes (Gibon
174 et al., 2004). The ratio of ATP maintenance cost to NADPH maintenance cost was
175 assumed to be 3:1 (Cheung et al., 2013) and maintenance costs were assumed to

be the same in the light and dark phases. In addition to the above constraints, fluxes through the chloroplastic NADPH dehydrogenase (NDH) and plastoquinol oxidase were set to zero as the contributions of NDH (Yamamoto et al., 2011) and plastoquinol oxidase (Josse et al., 2000) to photosynthesis are thought to be minor. The flux of sucrose synthase was constrained to be irreversible in the direction of sucrose degradation, as it is thought that sucrose synthase is not involved in sucrose synthesis in leaves (Nguyen-Quoc et al., 1990).

In order to maintain a metabolic output at night, the model must accumulate carbon and nitrogen stores during the day. To explore the metabolic interaction between the day and the night, the model included a set of sugars and carboxylic acids to be utilised as carbon storage molecules. Specifically, starch, glucose, fructose, malate, fumarate and citrate were free to accumulate during either the day or night phase. No direct constraints were applied to the amount of each compound that accumulated other than the requirement for the overall model to be mass balanced. For nitrogen, nitrate and the 20 common amino acids were allowed to accumulate as storage compounds, but the latter were constrained such that accumulation was only permitted during the day but not at night, in accordance with observations on the diel fluctuations of amino-acids in leaves (Scheible et al., 2000). Again, no direct constraints were applied to the amount of each amino acid to be accumulated. Thus the model was free to choose among a set of storage compounds to allow the constraint of export of sugars and amino acids at night to be met. The interconnections between the light and dark phases of the model, as well as the input and output constraints, are summarised in Fig. 1. Fluxes were predicted using linear programming with an objective function to minimise the sum of fluxes within the specified constraints. The two phases were modelled simultaneously in a single optimisation problem analogous to modelling interactions between two micro-organisms or two tissues/cell-types in multicellular organisms (de Oliveira Dal'Molin et al., 2010b). As Arabidopsis is a C_3 plant, the ratio of Rubisco carboxylation to oxygenase was set to a typical value of 3:1 to simulate photorespiration (Gutteridge and Pierce, 2006).

The integrated day-night model leads to altered flux predictions in comparison to a constant light model

To assess the effect of the diel modelling framework, fluxes predicted in the light phase of the diel model were compared to those predicted in a constant-light model. The latter model was constrained by total sucrose and amino-acid export and cellular maintenance costs that matched those over a 24-hour period in the diel model.

To take account of the fact that some fluxes are not uniquely defined at the optimum, flux variability analysis was used to determine the feasible range of all fluxes. Fluxes in the light component of the diel model were considered to be significantly different from those of the same reactions in the constant light models if their flux ranges did not overlap. This procedure identified 131 reactions with non-overlapping flux ranges in the light (Supplemental Table II). These reactions carried different fluxes in the light, but none carried flux in opposite directions in the two models. Fluxes were compared using a similarity measure calculated from the fraction of the smaller flux value over the larger flux value. Reactions with a similarity measure of less than 0.25 are listed in Table I, where the smaller the value of this measure, the larger the difference in fluxes. A similarity measure of zero means that the reaction carried zero flux in one of the models. Some reactions that carried different fluxes between the diel and constant light models are to be expected. For example, starch synthesis was turned on during the day in the diel model, but not in the constant light model where there was no need to store carbon because of the continuous assimilation of CO_2. Similarly transport of carboxylic acids and nitrate across the tonoplast for storage in the vacuole was activated in the diel model.

However, there were also changes in metabolic fluxes that were less directly constrained. These relate to the citrate used to provide carbon skeletons for glutamate and glutamine synthesis in the light. Table I shows that the synthesis of citrate was predicted to occur in the peroxisome via peroxisomal citrate synthase. In contrast, the diel model predicted that citrate would be synthesised via the mitochondrial TCA cycle during the night and stored in the vacuole. Nocturnally stored citrate was then exported from the vacuole during the day and metabolised into 2-oxoglutarate via aconitase and isocitrate dehydrogenase for glutamate synthesis (Fig. 2). The prediction of the diel model is consistent with observations from isotopic labelling experiments (Gauthier et al., 2010) and this example demonstrates the importance of considering the interconnections between light and dark metabolism for the prediction of realistic flux distributions.

Predictions of metabolic network fluxes in a mature C_3 leaf over a day-night cycle

The flux solution using the day-night modelling framework can be summarised in a simple flux map (Fig. 3) and a complete list of predicted flux ranges for reactions in the light and dark are provided in Supplemental Table III. The diurnal modelling framework successfully predicted that starch is the main carbon storage compound that accumulates in the light even though the model was free to utilise sugars and carboxylic acids as the carbon store. Some malate was also predicted to accumulate in the light, which then fed into the TCA cycle in the dark. Interestingly, the model predicted that both citrate and nitrate were stored at night in order to support nitrogen assimilation which was predicted to occur primarily during the day. The nitrate store was generated by transporting imported nitrate from the xylem into the vacuole during the night and release of the vacuolar store to the cytosol during the day. The model also predicted the storage during the day of a proportion of amino acids synthesised in the light and these were then exported into the phloem in the dark.

In the light phase, the model predicted large fluxes through the linear photosynthetic electron transport pathway and the Calvin-Benson pathway to support sucrose and amino acid synthesis and starch accumulation. The classical photorespiratory pathway for the oxidation of 2-phosphoglycolate was also predicted to be active due to a constraint in the model that set the Rubisco carboxylation to oxygenase ratio to 3:1. Note, that if this constraint is removed, the Rubisco oxygenase reaction become inactive. The TCA cycle was predicted to operate in a non-cyclic mode in the light with two separate branches (Fig. 4) consistent with the current understanding based on isotope labelling experiments, and as predicted from other flux-balance models (Sweetlove et al., 2010). Oxaloacetate produced from phospho*enol*pyruvate carboxylase was converted into malate which accumulated in the light. The model predicted that the mitochondrial electron transport chain (ETC) is active in the light, carrying a flux equivalent to 10% of the flux through photosynthetic linear electron transport. The mitochondrial ATP synthase was predicted to contribute to 18% of total ATP synthesis in the light with the rest produced by the chloroplast thylakoid ATP synthase. The two sources of NADH

feeding into the mitochondrial ETC are glycine decarboxylase and the malate-oxaloacetate shuttle (Fig. 5) with contributions of 53% and 47% respectively (the mitochondrial isocitrate dehydrogenase reaction is predicted to exclusively generate NADPH which is used for maintenance reactions in the mitochondrion). The ultimate source of reductant in a photosynthetic leaf is from the photosynthetic linear electron transport. While most of the reducing power is used for photosynthetic CO_2 fixation in the chloroplast, a small proportion of reductant was shuttled out of the chloroplast by the malate-OAA shuttle (11%) and the 3-phosphoglycerate (3PGA)-glyceraldehyde 3-phosphate (GAP) shuttle (4%) (Fig. 5). Malate-OAA exchanges were responsible for transfer of reductant from the chloroplast into the cytosol, the mitochondrion and the peroxisome. The 3PGA-GAP shuttle transported reductant from the chloroplast to the cytosol to produce NADPH by the non-phosphorylating NADP-GAPDH. A proportion of NADPH produced in the cytosol was shuttled into the mitochondrion by the isocitrate-2-oxoglutarate shuttle (Fig. 5).

In the dark phase, the largest fluxes are related to starch degradation, sucrose synthesis, glycolysis, the oxidative pentose phosphate pathway (OPPP), the TCA cycle and the mitochondrial electron transport chain (Fig. 3). The breakdown of starch was predicted to be carried out by the hydrolytic pathway generating maltose for transport from the chloroplast to the cytosol. This is the result of constraining the chloroplastic hexose phosphate transporter to carry zero flux, in line with experimental observations (Niewiadomski et al., 2005), thus limiting the possible metabolic routes for carbon export from the chloroplast. When this constraint was removed starch breakdown occurred via starch phosphorylase. Glycolysis and the OPPP were predicted to occur in both the cytosol and the chloroplast, with 72% of the total flux through glycolytic glyceraldehyde 3-phosphate dehydrogenase and 55% of that through the OPPP glucose 6-phosphate dehydrogenase steps occurring in the cytosol. The TCA cycle operates in a cyclic mode in the dark (Fig. 4) consuming pyruvate produced from stored starch via glycolysis. A small proportion of the citrate produced by citrate synthase (15%) is stored in the dark to provide carbon skeletons for glutamate and glutamine synthesis in the light.

Predictions of metabolic fluxes in a mature CAM leaf over a diurnal cycle

From a structural metabolic modelling perspective, the Arabidopsis genome-scale metabolic model contains all the metabolic reactions required to carry out the various subtypes of CAM photosynthesis. However, because the metabolic cycle that constitutes CAM photosynthesis is temporally segregated, metabolism in CAM leaves cannot be modelled with a single-steady state FBA model. We therefore applied the diel modelling framework to predict metabolic fluxes in a mature CAM leaf over a 24-hour cycle. As for the mature C_3 leaf, the model was constrained by sucrose and amino acid export and cellular maintenance costs. The main additional constraint for simulating CAM photosynthesis was that CO_2 exchange with the environment was set to have zero flux in the light to simulate the closure of stomata in CAM plants during the day. Other differences between the C_3 and CAM models arose from the treatment of the Rubisco oxygenase activity and the export of carbon from the plastids. First, Rubisco oxygenase activity is likely to be suppressed in CAM leaves in the light due to the increase in the internal partial pressure of CO_2, but since there is also an increase in internal oxygen concentration, it is unclear to what extent photorespiration is prevented in CAM plants (Lüttge, 2011). Accordingly the Rubisco carboxylase to oxygenase ratio was left unconstrained in the light phase of the CAM model. Secondly, in the ice plant *Mesembryanthemum crystallinum* L., a facultative CAM plant, chloroplasts of CAM-induced plants mainly export glucose 6-phosphate (Neuhaus and Schulte, 1996) and this is coincident with a 71-fold increase in transcript level for the chloroplastic G6P transporter (Cushman et al., 2008). On this basis, the chloroplastic glucose 6-phosphate transporter was not constrained in the CAM model. Finally the various subtypes of CAM photosynthesis were simulated by setting the reactions specific to other subtypes to carry zero flux. The constraints applied for modelling the different modes of photosynthesis are summarised in Table II.

Using the diel modelling framework with CAM-specific constraints, FBA successfully predicted metabolic fluxes consistent with the well-known CAM cycle (Supplemental Table III). In the light, nocturnally stored malate was decarboxylated by malic enzyme or PEPCK depending on the subtype. In the generic CAM model (no sub-type constraints), 89% of malate decarboxylation was predicted to be carried out by PEPCK, with the remaining 11% carried out by the cytosolic malic enzyme. In addition to the photosynthetic linear electron transport and reductive pentose phosphate pathway, which were expected to carry high fluxes in the light, the

gluconeogenesis pathway also carried a high predicted flux in the light to convert PEP, from malate decarboxylation, to starch or soluble sugars for storage as part of the CAM cycle. In the generic CAM model, only starch was stored during the day but not soluble sugars. In our initial models of the sugar-storing subtypes, fructose was produced in the cytosol by sucrose synthase and subsequently transported into the vacuole by the vacuolar hexose transporter. However, it is thought that tonoplast hexose transport activity is restricted to the night (in an efflux capacity) in CAM plants to avoid futile cycling (Holtum et al., 2005; Antony et al., 2008). When the vacuolar hexose transporter activity was subsequently restricted to the dark period, the model predicted that sucrose is imported into the vacuole and catabolised into glucose and fructose by vacuolar invertase, which is in line with postulated models in the literature (Smith and Bryce, 1992; McRae et al., 2002; Holtum et al., 2005).

The Rubisco carboxylase to oxygenase ratio was unconstrained in modelling CAM and the model predicted no Rubisco oxygenase flux suggesting that Rubisco oxygenase is not necessary for the functioning of a mature CAM leaf under the assumption of minimising total flux. The mitochondrial ETC and ATP synthase carried high fluxes in the light with the mitochondrial ETC carrying a flux equivalent to 29% of the flux through photosynthetic linear electron transport and the mitochondrial ATP synthase contributing to 34% of the total ATP produced in the light in the generic CAM model. Similar values were predicted for the various CAM subtypes. Similar to C_3 leaves, an incomplete TCA cycle was predicted in the light phase with two separate branches, citrate to 2-oxoglutarate and succinate to oxaloacetate (Fig. 6). Interestingly, the oxaloacetate-branch differed from that found for the C_3 model in that oxaloacetate was produced, not consumed and succinate was the starting point of the branch, not fumarate (Figs. 4 and 6). In the CAM TCA cycle, the two branches are joined via the activity of isocitrate lyase in the peroxisome to produce succinate (Fig. 6).

In the dark phase, the stored carbon (starch or soluble sugars) was predicted to be catabolised to produce PEP, the substrate for carboxylation, via glycolysis. PEP was carboxylated by PEP carboxylase to produce oxaloacetate, which was subsequently converted into malate for storage in the vacuole as malic acid during the night. With respect to starch degradation, the phosphorolytic route via starch phosphorylase was predicted in CAM because it is more energetically efficient than the hydrolytic route via maltose, and this is consistent with the current view of the

CAM cycle (Weise et al., 2011). While most of the carbon store was used to provide the substrate for carboxylation in the CAM cycle, some went into the OPPP, to produce NADPH for maintenance processes, and into the TCA cycle, to produce NADH for ATP synthesis via the mitochondrial ETC and ATP synthase. As in a mature C_3 leaf, the model predicted a complete TCA cycle in the dark in a mature CAM leaf (Fig. 6).

Quantitative comparisons of metabolism between C_3 and CAM leaves

The CO_2-concentrating mechanism in CAM is an energy-requiring process and the energetic cost of supporting sucrose and amino acid export from mature leaves and cell maintenance processes was compared between C_3 and CAM in terms of photon use (Fig. 7). Photon use in a mature CAM leaf is similar to that in a C_3 leaf, being ±10% of C_3 depending on the CAM subtype.

Rubisco is the most abundant protein on earth, contributing up to 50% of the soluble protein and 20-30% of the total nitrogen in a C_3 leaf (Feller et al., 2008). The investment in Rubisco, in terms of energy and nitrogen, is likely to contribute significantly to the evolutionary fitness trade-off in plants. By comparing the model predictions, it was apparent that total flux through Rubisco (carboxylase + oxygenase flux) was lower in CAM than C_3, mainly as a consequence of the prediction of no oxygenase activity in the CAM model (Fig. 7). While this may suggest a cost-saving for a CAM plant, it is offset by the fact that the CO_2-concentrating mechanism requires high fluxes through the CAM cycle. As a consequence, the total flux through the entire metabolic network is 32-64% higher in CAM than in C_3 (Fig. 7).

DISCUSSION

Integration of light and dark metabolism is required to capture known features of leaf metabolism by FBA

The usefulness of constraints-based modelling tools such as FBA depends on the extent to which they capture known features of the metabolic network. Good agreement has been reported between the predicted and measured fluxes for a heterotrophic Arabidopsis cell culture, leading to insights into cell maintenance costs

under stress conditions (Cheung et al., 2013). There is an expectation that a similar modelling approach will be useful in analysing photosynthetic metabolism, but most applications to date have been based on the analysis of the network under conditions of constant light. Here analysis of the Arabidopsis model revealed that there are several features of leaf metabolism that can only be captured by FBA by considering the interaction between the temporally-separated phases of light and dark metabolism. For example, the diel model accumulated citrate in the vacuole during the night and this was released during the day to provide carbon skeletons for nitrogen assimilation. This agrees with evidence from isotope labelling experiments (Gauthier et al., 2010) and the current view of carboxylic acid metabolism in leaves in the light (Tcherkez et al., 2009; Sweetlove et al., 2010). In contrast, a single-steady-state, constant light FBA leaf model generated citrate via an unusual metabolic route involving threonine aldolase and peroxisomal citrate synthase. This route is most likely chosen by the model because of its efficiency in terms of carbon use: the route leads to the fixation of 1 CO_2 by PEP carboxylase and releases 0.5 CO_2 from the recycling of glycine via the photorepiratory pathway. In another Arabidopsis genome-scale metabolic model, the threonine aldolase reaction was absent and the model predicted that citrate would be synthesised from pyruvate by pyruvate dehydrogenase and mitochondrial citrate synthase (de Oliveira Dal'Molin et al., 2010a), contradicting well-established evidence that the mitochondrial pyruvate dehydrogenase is inhibited transcriptionally and post-transcriptionally in leaves in the light (Tovar-Mendez et al., 2003).

A possible explanation for the accumulation of citrate in the dark over the synthesis of citrate from primary photosynthate in the light could be that the degradation of starch to produce citrate (via glycolysis, PEP carboxylase, pyruvate dehydrogenase and citrate synthase) provides a carbon-neutral route for transferring ATP and reducing power from the light phase to the dark phase. This conserves the net carbon required to support dark metabolism, where citrate in the dark would otherwise be metabolised through the TCA cycle and the carbon would be released as CO_2. Confirming this, if the model was configured with citrate accumulation prevented, the total CO_2 release in the dark was increased by 2%.

The diel model was free to choose between a range of carbon- (starch, sugars and carboxylic acids) and nitrogen-storage compounds (nitrate and amino acids) to support the export of sugars and amino acids during the night, and to meet

447 the night-time maintenance costs. The fact that the model solution selected starch
448 and amino acids as the main daytime storage carbon and nitrogen compounds,
449 respectively, consistent with the known biochemistry of C_3 leaves, reflects the
450 success of the objective function (minimisation of sum of fluxes) in capturing the
451 drivers that shape the metabolic system. Essentially, the choice of starch over
452 sugars and amino acids over nitrate storage, leads to a more efficient metabolic
453 network. For example, it is energetically less costly to mobilise a plastidic starch
454 store than a vacuolar sucrose store. Leaf starch breakdown initially occurs
455 hydrolytically in the plastid to generate maltose which is then metabolised to hexose
456 phosphate by a combination of the cytosolic enzymes glucosyltransferase,
457 hexokinase and α-glucan phosphorylase (Zeeman et al., 2004). The latter enzyme
458 uses Pi rather than ATP as the phosphoryl donor, and hence saves an ATP
459 compared to the breakdown of vacuolar sucrose via invertase and phosphorylation
460 by hexokinases. The choice of starch over carboxylic acids is again driven by the
461 efficiency driver of the objective function: carboxylic acids are more oxidised than
462 starch and hence the energy stored per carbon is less than for starch. The model
463 also correctly predicted that nitrate assimilation would occur only during the day, it
464 being overall more efficient (lower sum of fluxes) to store nitrate that is imported into
465 the leaf at night and release it from the vacuole (along with appropriate quantities of
466 citrate) during the day for assimilation into amino acids, consistent with experimental
467 measurements (Stitt et al., 2002).
468 However, it should be noted that the behaviour of all these models is highly
469 dependent on the accuracy of the reaction list and the nature of the constraints
470 applied. The choice of objective function will also affect the flux solution, although we
471 have previously demonstrated that the choice of objective function is less important
472 than the constraints applied to an FBA model of heterotrophic metabolism (Cheung
473 et al., 2013). Similarly, for this model, the use of other objective functions (e.g.
474 minimisation of photon use) did not change the main conclusions about the operation
475 of the network through the diel cycle. Having established that the diel modelling
476 framework can capture realistic aspects of leaf metabolism through the day-night
477 cycle, it can be employed in future to examine how the predicted flux distribution
478 changes in response to different metabolic scenarios such as variations in available
479 light for photosynthesis and the transition from sink to source leaves.
480

The diel metabolic modelling framework allows simulation and analysis of CAM

The diel framework for FBA also allows CAM photosynthesis to be tackled for the first time. Only minimal changes to the constraints of the diel C_3 model were required to capture the classical CAM cycle, the major change being to constrain CO_2 exchange with the environment to zero during the light. This constraint forced the model to carry out net carbon fixation during the night. Even though the model was set up with free choices for the use of carboxylating enzymes and the nocturnal carbon store (from malate, fumarate, citrate, starch and soluble sugars), the conventional CAM cycle was predicted with PEP carboyxlase as the carboxylating enzyme and malate as the main temporary storage of fixed carbon in the dark. In addition to malate, a small amount of citrate was predicted to accumulate during the night, and this was used during the day in part to support nitrate assimilation and in part for conversion to malate via isocitrate lyase. In fact, some CAM plants accumulate a large amount of citrate during the night (Lüttge, 1988; Borland and Griffiths, 1988) and it has been speculated that either ATP citrate lyase or the TCA cycle are used for catabolism of this stored citrate (Holtum et al., 2005). ATP citrate lyase produces oxaloacetate and acetyl-CoA from citrate, but since there is no major sink for acetyl-CoA in the output constraints, this route was not chosen by the model. One possible reason for preferring isocitrate lyase over the TCA cycle is that the conversion of citrate to malate by the former route releases less CO_2 per molecule of citrate (glyoxylate produced from isocitrate lyase is metabolised through the photorespiratory pathway, producing 0.5 molecules of 3PGA and 0.5 molecules of CO_2 per molecule of citrate catabolised) than the latter route (2 molecules of CO_2 released per molecule of citrate catabolised by aconitase, isocitrate dehydrogenase and 2-oxoglutarate dehydrogenase). In the absence of measurements of ATP citrate lyase and isocitrate lyase in CAM plants, it is not clear whether these two enzymes are involved in the catabolism of citrate in vivo. Transcripts for both enzymes were identified in a recent sequencing study of two agave species (Gross et al., 2013) but at present, there is no quantitative data on the expression or activity levels that could be used to discriminate between the possible routes. Ultimately, detailed metabolic flux analysis would be required to examine this issue.

Analysis of the energetics of CAM metabolism

In the model of CAM leaf metabolism, where the model was free to choose between different decarboxylating enzymes and storage compounds, malate decarboxylation was predicted to be mainly carried out by PEPCK. This can be explained by the observation that the mPEPCK-subtypes of CAM require fewer photons, which leads to a lower total flux through the metabolic network (the objective function that is optimised in the model) than the ME-subtypes (Fig. 7). In other words, considering the whole network, the PEPCK-subtype is more energetically efficient. This conclusion contrasts with previous manual calculations of CAM-subtype energetics that considered the stoichiometry of a much smaller metabolic network (Winter and Smith, 1996) and emphasises that the net balance of ATP and NAD(P)H consumption is a property of the whole network.

While CAM undoubtedly represents an adaptation to arid conditions (Cushman, 2001; Silvera et al., 2010), the CAM cycle also acts as a CO_2-concentrating mechanism and reduced CO_2 availability may have been the common, original selection pressure that led to the evolution of CAM in both terrestrial and aquatic environments (Keeley and Rundel, 2003). The CO_2 concentrating mechanism may also supress the carbon- and energy-consuming process of photorespiration, although this is open to debate and depends critically upon the internal CO_2:O_2 concentration ratio. However, there is a trade-off between the energetic investment in the CO_2-concentrating mechanism in the form of the CAM cycle and the benefit of suppressing photorespiration. The modelling results suggest that the photon use of C_3 and CAM leaves are similar (Fig. 7), meaning that there is little to be gained in terms of energetics in running the CAM cycle. However as well as the running costs of the network, there is also the cost of the enzyme machinery. A knock-on consequence of suppression of Rubisco oxygenase activity is that less Rubisco protein is required to fix a given amount of carbon. Given that Rubisco contributes up to 50% of the soluble proteins and 20-30% of the total nitrogen in a C_3 leaf (Feller et al., 2008), the predicted reduction of 22-32% of total Rubisco flux in CAM compared to C_3 could be a significant benefit in terms of nitrogen use efficiency. However, at the same time, there are additional enzyme machinery costs for operating the CAM cycle. There are contradicting experimental observations relating to nitrogen efficiency in CAM plants (Luttge, 2004). From the model

549 predictions, CAM requires 12-43% more total flux through the metabolic network
550 than C_3. Although enzyme machinery cost per metabolic flux for each reaction will
551 vary depending on factors such as the size and the turnover rate of the enzyme, the
552 total network flux can be used as a proxy for the overall enzyme machinery cost by
553 averaging out the variation between reactions, although the extent to which this
554 assumption is distorted by very abundant enzymes with low K_{cat} values, such as
555 Rubisco, has not been tested. By balancing the benefit from reduced Rubisco
556 requirement with the increase in enzyme machinery costs in the rest of the metabolic
557 network, the total nitrogen invested in enzyme machinery is likely to be similar in C_3
558 and in CAM. Thus the modelling results suggest that energetics and nitrogen use
559 efficiency are unlikely to have been contributory drivers for the evolution of CAM
560 photosynthesis.
561
562 **CONCLUSION**
563
564 The diel FBA-modelling framework not only predicted known features of leaf
565 metabolism more accurately than a continuous light model, but it also allowed CAM
566 photosynthesis to be modelled at a network scale. This has allowed an accurate
567 accounting of the energetics of CAM metabolism, demonstrating that there are
568 unlikely to be substantial energetic benefits in CAM photosynthesis over C_3, despite
569 the potential for suppression of photorespiration due to the CO_2-concentrating effect
570 of the CAM cycle. In the current diel FBA framework it is assumed that the light and
571 dark phase each represent pseudo steady-states. This ignores known differences in
572 metabolic behaviour that occur within each phase, particularly at the light-dark
573 transition points, in both C_3 and CAM leaves. The framework can easily be extended
574 to account for such transitions, by further sub-dividing each phase. However, this
575 requires a more detailed knowledge of the input-output constraints at each time-step
576 and will lead to a more tightly constrained model where each time step is solved as
577 an independent or concatenated FBA problem. For this initial exploration, it was
578 preferable to apply minimal constraints to establish whether a metabolic network
579 optimised for efficiency (lowest overall flux) matched known configurations of C_3 and
580 CAM metabolism over a diel cycle.
581
582 **MATERIALS AND METHODS**

Construction of a diel metabolic model

The genome-scale metabolic model of Arabidopsis used for the analysis of heterotrophic metabolism (Cheung et al., 2013) was adapted to model leaf metabolism over a day-night cycle. The diel modelling framework was developed by dividing the day-night cycle into two phases, light and dark, with metabolism in each phase assumed to be at steady-state. The model was constructed by duplicating the Arabidopsis genome-scale metabolic model, with the reactions and metabolites in each duplicate labelled "_Light" or "_Dark" before the compartmentation suffix. In addition, dummy reactions for "transporting" storage metabolites from one phase to another were manually added with the suffix "_LightDark". The diel model is available in SBML format (Supplementary Data 1). Flux balance analysis and flux variability analysis were implemented as before (Cheung et al., 2013).

Quantitative comparison between flux ranges calculated from the diel model and the continuous light model

Flux ranges for reactions in the light were calculated using flux variability analysis for the diel model, (v_{min}^{diel},v_{max}^{diel}), and the continuous light model, (v_{min}^{single}, v_{max}^{single}). Reversible reactions carrying fluxes in opposite directions in the two sets of flux ranges were defined as reactions where either $v_{min}^{diel} \geq 0$ and $v_{max}^{single} \leq 0$ or $v_{min}^{single} \geq 0$ and $v_{max}^{diel} \leq 0$. Reactions with non-overlapping flux ranges were defined as reactions where either $v_{min}^{diel} > v_{max}^{single}$ or $v_{min}^{single} > v_{max}^{diel}$). For reactions with non-overlapping flux ranges that did not carry fluxes in opposite directions, a similarity measure was calculated as $v_{max}^{low}/v_{min}^{high}$, where v_{max}^{low} is the maximum flux of the reaction with the lower flux range of the pair and v_{min}^{high} is the minimum flux of the reaction with the higher flux range. This measure varies from 0 to 1 where a value close to 0 represents a large difference between the flux ranges.

Supplemental Data

Supplemental Table I. Relative amino-acid composition in the phloem of Arabidopsis.

Supplemental Table II. List of reactions with non-overlapping flux ranges between the diel model and the single steady-state model and their similarity measures.

Supplemental Table III. Predicted fluxes for reactions in the light and the dark in a leaf with either C3 or CAM photosynthesis.

Supplemental Data 1. Diel model of Arabidopsis leaf metabolism in SBML format.

ACKNOWLEDGEMENTS

We would like to thank Professor J.A.C. Smith (University of Oxford) for discussions on the energetics of CAM metabolism.

LITERATURE CITED

Antony E, Taybi T, Courbot M, Mugford ST, Smith JAC, Borland AM (2008) Cloning, localization and expression analysis of vacuolar sugar transporters in the CAM plant *Ananas comosus* (pineapple). J Exp Bot **59:** 1895-1908

Borland AM, Griffiths H (1989) The regulation of citric acid accumulation and carbon recycling during CAM in *Ananas comosus*. J Exp Bot **40:** 53-60

Boyle NR, Morgan JA (2009) Flux balance analysis of primary metabolism in *Chlamydomonas reinhardtii*. BMC Syst Biol **3:** 4

Cheung CYM, Williams TCR, Poolman MG, Fell DA, Ratcliffe RG, Sweetlove LJ (2013) A method for accounting for maintenance costs in flux balance analysis improves the prediction of plant cell metabolic phenotypes under stress conditions. Plant J **75:** 1050-1061

Cushman JC (2001) Crassulacean acid metabolism. A plastic photosynthetic adaptation to arid environments. Plant Physiol **127:** 1439-1448

Cushman JC, Tillett RL, Wood JA, Branco JM, Schlauch KA (2008) Large-scale mRNA expression profiling in the common ice plant, *Mesembryanthemum*

crystallinum, performing C_3 photosynthesis and Crassulacean acid metabolism (CAM). J Exp Bot **59:** 1875-1894

de Oliveira Dal'Molin CG, Quek LE, Palfreyman RW, Brumbley SM, Nielsen LK (2010a) AraGEM, a genome-scale reconstruction of the primary metabolic network in Arabidopsis. Plant Physiol **152:** 579-589

de Oliveira Dal'Molin CG, Quek LE, Palfreyman RW, Brumbley SM, Nielsen LK (2010b) C4GEM, a genome-scale metabolic model to study C_4 plant metabolism. Plant Physiol **154:** 1871-1885

de Oliveira Dal'Molin CG, Quek LE, Palfreyman RW, Nielsen LK (2011) AlgaGEM - a genome-scale metabolic reconstruction of algae based on the *Chlamydomonas reinhardtii* genome. BMC Genomics **12 (Suppl 4):** S5

Delhon P, Gojon A, Tillard P, Passama L (1995) Diurnal regulation of NO_3^- uptake in soybean plants.1. Changes in NO_3^- influx, efflux, and N utilization in the plant during the day/night cycle. J Exp Bot **46:** 1585-1594

Feller U, Anders I, Mae T (2008) Rubiscolytics: fate of Rubisco after its enzymatic function in a cell is terminated. J Exp Bot **59:** 1615-1624

Gauthier PPG, Bligny R, Gout E, Mahé A, Nogués S, Hodges M, Tcherkez GGB (2010) *In folio* isotopic tracing demonstrates that nitrogen assimilation into glutamate is mostly independent from current CO_2 assimilation in illuminated leaves of *Brassica napus*. New Phytol **185:** 988-999

Gibon Y, Bläsing OE, Palacios-Rojas N, Pankovic D, Hendriks JHM, Fisahn J, Höhne M, Günther M, Stitt M (2004) Adjustment of diurnal starch turnover to short days: depletion of sugar during the night leads to a temporary inhibition of carbohydrate utilization, accumulation of sugars and post-translational activation of ADP-glucose pyrophosphorylase in the following light period. Plant J **39:** 847-862

Gross SM, Martin JA, Simpson J, Abraham-Juarez MJ, Wang Z, Visel A (2013) *De novo* transcriptome assembly of drought tolerant CAM plants, *Agave deserti* and *Agave tequilana*. BMC Genomics **14:** 563

Gutteridge S, Pierce J (2006) A unified theory for the basis of the limitations of the primary reaction of photosynthetic CO2 fixation: Was Dr. Pangloss right? Proc Natl Acad Sci USA **103:** 7203-7204

Hay J, Schwender J (2011) Computational analysis of storage synthesis in developing *Brassica napus* L. (oilseed rape) embryos: flux variability analysis in relation to ^{13}C metabolic flux analysis. Plant J **67:** 513-525

Holtum JAM, Smith JAC, Neuhaus HE (2005) Intracellular transport and pathways of carbon flow in plants with crassulacean acid metabolism. Funct Plant Biol **32:** 429-449

Josse EM, Simkin AJ, Gaffe J, Laboure AM, Kuntz M, Carol P (2000) A plastid terminal oxidase associated with carotenoid desaturation during chromoplast differentiation. Plant Physiol **123:** 1427-1436

Keeley JE, Rundel PW (2003) Evolution of CAM and C_4 carbon-concentrating mechanisms. Int J Plant Sci **164:** S55-S77

Knoop H, Gründel M, Zilliges Y, Lehmann R, Hoffmann S, Lockau W, Steuer R (2013) Flux balance analysis of cyanobacterial metabolism: the metabolic network of Synechocystis sp. PCC 6803. PLoS Comput Biol **9:** e1003081

Knoop H, Zilliges Y, Lockau W, Steuer R (2010) The metabolic network of Synechocystis sp. PCC 6803: systemic properties of autotrophic growth. Plant Physiol **154:** 410-422

Kramer DM, Evans JR (2011) The importance of energy balance in improving photosynthetic productivity. Plant Physiol **155:** 70-78

Lüttge U (1988) Day-night changes of citric-acid levels in crassulacean acid metabolism: phenomenon and ecophysiological significance. Plant Cell Environ **11:** 445-451

Lüttge U (2004) Ecophysiology of crassulacean acid metabolism (CAM). Ann Bot **93:** 629-652

Lüttge U (2011) Photorespiration in phase III of crassulacean acid metabolism: evolutionary and ecophysiological implications. Prog Bot **72:** 371-384

Macduff JH, Bakken AK (2003) Diurnal variation in uptake and xylem contents of inorganic and assimilated N under continuous and interrupted N supply to *Phleum pratense* and *Festuca pratensis*. J Exp Bot **54:** 431-444

Maurino VG, Weber AP (2013) Engineering photosynthesis in plants and synthetic microorganisms. J Exp Bot **64:** 743-751

McRae SR, Christopher JT, Smith JAC, Holtum JAM (2002) Sucrose transport across the vacuolar membrane of *Ananas comosus*. Funct Plant Biol **29:** 717-724

Montagud A, Navarro E, Fernandez de Cordoba P, Urchueguia JF, Patil KR (2010) Reconstruction and analysis of genome-scale metabolic model of a photosynthetic bacterium. BMC Syst Biol **4:** 156

Neuhaus HE, Schulte N (1996) Starch degradation in chloroplasts isolated from C_3 or CAM (crassulacean acid metabolism)-induced *Mesembryanthemum crystallinum* L.. Biochem J **318:** 945-953

Nguyen-Quoc B, Krivitzky M, Huber SC, Lecharny A (1990) Sucrose synthase in developing maize leaves: regulation of activity by protein level during the import to export transition. Plant Physiol **94:** 516-523

Niewiadomski P, Knappe S, Geimer S, Fischer K, Schulz B, Unte US, Rosso MG, Ache P, Flügge UI, Schneider A (2005) The Arabidopsis plastidic glucose 6-

749 phosphate/phosphate translocator GPT1 is essential for pollen maturation and
750 embryo sac development. Plant Cell **17:** 760-775
751
752 **Nogales J, Gudmundsson S, Knight EM, Palsson BO, Thiele I** (2012) Detailing
753 the optimality of photosynthesis in cyanobacteria through systems biology analysis.
754 Proc Natl Acad Sci USA **109:** 2678-2683
755
756 **Poolman MG, Kundu S, Shaw R, Fell DA** (2013) Responses to light intensity in a
757 genome-scale model of rice metabolism. Plant Physiol **162:** 1060-1072
758
759 **Saha R, Suthers P, Maranas C** (2011) *Zea mays* i RS1563: a comprehensive
760 genome-scale metabolic reconstruction of maize metabolism. PloS ONE **6:** e21784
761
762 **Saha R, Verseput AT, Berla BM, Mueller TJ, Pakrasi HB, Maranas CD** (2012)
763 Reconstruction and comparison of the metabolic potential of cyanobacteria
764 *Cyanothece* sp. ATCC 51142 and *Synechocystis* sp. PCC 6803. PLoS ONE **7:**
765 e48285
766
767 **Scheible WR, Krapp A, Stitt M** (2000) Reciprocal diurnal changes of
768 phosphoenolpyruvate carboxylase expression and cytosolic pyruvate kinase, citrate
769 synthase and NADP-isocitrate dehydrogenase expression regulate organic acid
770 metabolism during nitrate assimilation in tobacco leaves. Plant Cell Environ **23:**
771 1155-1167
772
773 **Siebrecht S, Herdel K, Schurr U, Tischner R** (2003) Nutrient translocation in the
774 xylem of poplar - diurnal variations and spatial distribution along the shoot axis.
775 Planta **217:** 783-793
776
777 **Silvera K, Neubig KM, Whitten WM, Williams NH, Winter K, Cushman JC** (2010)
778 Evolution along the crassulacean acid metabolism continuum. Funct Plant Biol **37:**
779 995-1010
780

781 **Smith JAC, Bryce JH** (1992) Metabolite compartmentation and transport in CAM
782 plants. In AK Tobin, ed, Plant organelles. Cambridge University Press, Cambridge,
783 pp 141-167
784
785 **Stitt M, Muller C, Matt P, Gibon Y, Carillo P, Morcuende R, Scheible WR, Krapp**
786 **A** (2002) Steps towards an integrated view of nitrogen metabolism. J Exp Bot **53:**
787 959-970
788
789 **Sweetlove LJ, Beard KFM, Nunes-Nesi A, Fernie AR, Ratcliffe RG** (2010) Not
790 just a circle: flux modes in the plant TCA cycle. Trends Plant Sci **15:** 462-470
791
792 **Sweetlove LJ, Ratcliffe RG** (2011) Flux-balance modelling of plant metabolism.
793 Front Plant Sci **2:** 38
794
795 **Szecowka M, Heise R, Tohge T, Nunes-Nesi A, Vosloh D, Huege J, Feil R, Lunn**
796 **J, Nikoloski Z, Stitt M, Fernie AR, Arrivault S** (2013) Metabolic fluxes in an
797 illuminated Arabidopsis rosette. Plant Cell **25:** 694-714
798
799 **Tcherkez G, Mahe A, Gauthier P, Mauve C, Gout E, Bligny R, Cornic G, Hodges**
800 **M** (2009) *In folio* respiratory fluxomics revealed by ^{13}C isotopic labeling and H/D
801 isotope effects highlight the noncyclic nature of the tricarboxylic acid "cycle" in
802 illuminated leaves. Plant Physiol **151:** 620-630
803
804 **Tovar-Mendez A, Miernyk JA, Randall DD** (2003) Regulation of pyruvate
805 dehydrogenase complex activity in plant cells. Eur J Biochem **270:** 1043-1049
806
807 **Weise SE, van Wijk KJ, Sharkey TD** (2011) The role of transitory starch in C_3,
808 CAM, and C_4 metabolism and opportunities for engineering leaf starch accumulation.
809 J Exp Bot **62:** 3109-3118
810
811 **Wilkinson TL, Douglas AE** (2003) Phloem amino acids and the host plant range of
812 the polyphagous aphid, *Aphis fabae*. Entomol Exp Appl **106:** 103-113
813

Winter K, Smith JACS (1996) Crassulacean acid metabolism: current status and perspectives. In K Winter, JACS Smith, eds, Crassulacean acid metabolism. Biochemistry, ecophysiology and evolution. Springer-Verlag, Berlin, pp 389-426

Yamamoto H, Peng LW, Fukao Y, Shikanai T (2011) An Src homology 3 domain-like fold protein forms a ferredoxin binding site for the chloroplast NADH dehydrogenase-like complex in *Arabidopsis*. Plant Cell **23:** 1480-1493

Yan XY, Tan DKY, Inderwildi OR, Smith JAC, King DA (2011) Life cycle energy and greenhouse gas analysis for agave-derived bioethanol. Energy Environ Sci **4:** 3110-3121

Zeeman SC, Smith SM, Smith AM (2004) The breakdown of starch in leaves. NewPhytol **163:** 247-261

FIGURE LEGENDS

Figure 1. Flux-balance framework for integrated metabolic modelling of the day and night phases of a mature leaf. The light dark phases are represented by the white and grey backgrounds of the diagram respectively. Metabolites shown in the dashed rectangles between the two phases represent potential storage compounds. Starch, glucose, fructose, malate, fumarate, citrate and nitrate were allowed to accumulate in the light and in the dark as denoted by the arrows pointing towards the light and dark states. Twenty common amino-acids were allowed to accumulate in the light but not in the dark as denoted by the arrow pointing from the light phase to the dark phase. Export to the phloem was set to four sucrose to one amino-acid, with 18 different amino-acids in the proportions shown in Supplemental Table 1.The export rate was set to be three times greater in the light that in the dark. Nitrate was set as the sole nitrogen source with the ratio of nitrate uptake from the phloem in the light to that in the dark set to 3 to 2. Cellular maintenance costs in the dark were set to a fixed value where the carbon exported during the night roughly equalled the carbon released as CO_2 in the dark phase. Maintenance costs were assumed to be the same in the light and the dark. The ratio of ATP maintenance cost to NADPH maintenance cost was set to 3 to 1.

Figure 2. Metabolic routes for glutamate biosynthesis from two modelling approaches. A single steady-state model in constant light is shown on the left and the diel modelling framework on the right. In constant light, the carbon skeletons for glutamine synthesis were predicted to be supplied via a metabolic route in which threonine is metabolised in the cytosol to acetate, transported to the peroxisome and metabolised to citrate which is exported to the cytosol and converted to 2-oxoglutarate. Using the diel modelling framework, the model predicted the use of citrate stored in the dark to provide the carbon skeletons for glutamate synthesis in the light. Abbreviations: PEP, phospho*enol*pyruvate; OAA oxaloacetate. The thickness of the arrows is scaled to indicate relative flux magnitudes (in molar units).

Figure 3. Predicted flux map of metabolism for a mature C_3 leaf over a day-night cycle. The light dark phases are represented by the white grey backgrounds respectively. Metabolites shown in the dashed rectangles between the two phases

represent storage compounds. The thickness of the arrows is proportional to the metabolic flux through the reactions (in molar units). Metabolic processes listed within rounded rectangles carry fluxes too large to be represented on the flux map. Abbreviations: ETC, electron transport chain; OPPP, oxidative pentose phosphate pathway; TCA, tricarboxylic acid.

Figure 4. Flux predictions through the TCA cycle and pyruvate dehydrogenase in a C_3 leaf in the light and the dark. A non-cyclic mode with two separate branches, citrate to 2-oxoglutarate and oxaloacetate and fumarate to malate, was predicted to operate in the light. A cyclic mode of the TCA cycle was predicted to operate in the dark, mainly to produce ATP via oxidative phosphorylation. Fluxes illustrated are net conversion between metabolites over all subcellular compartments. The thickness of the arrows is proportional to the metabolic fluxes through the reactions (in molar units). Citrate stored in the dark is represented by an arrow pointing from the dark phase to the light phase. Malate storage is not illustrated in this diagram.

Figure 5. Reductant shuttling between subcellular compartments and the production and consumption of NADH in mitochondria in the light. Left-pointing arrows represent reductant-consuming reactions; right-pointing arrows represent reductant-producing reactions. The thickness of the solid arrows is proportional to the metabolic flux through the reactions (in molar units), except for the conversion between 3PGA and GAP in the chloroplast where the zig-zag line across the arrow indicates that the flux is too large to be illustrated to scale in the diagram. Reductant shuttles between four subcellular compartments, cytosol, chloroplast, mitochondria and peroxisome, are shown with dashed arrows representing transfer of metabolites between compartments. Abbreviations: 2OG, 2-oxoglutarate; 3PGA, 3-phosphoglycerate; ETC, electron transport chain; GAP, glyceraldehyde 3-phosphate; OAA, oxaloacetate.

Figure 6. Flux predictions through the TCA cycle and related reactions in a CAM leaf. A non-cyclic mode with two distinct branches, citrate to 2-oxoglutarate and succinate to oxaloacetate, was predicted to operate in the light. The two branches of the TCA cycle are connected by isocitrate lyase which converts isocitrate into succinate and glyoxylate. A cyclic mode of the TCA cycle was predicted to operate in

897 the dark, mainly to contribute to ATP production via oxidative phosphorylation.
898 Fluxes illustrated are net conversion between metabolites over all subcellular
899 compartments. The thickness of the arrows is proportional to the metabolic flux
900 through the reactions (in molar units), except for the conversion between malate and
901 oxaloacetate where the zig-zag line across the arrow indicates that the flux is too
902 large to be illustrated to scale in the diagram. Citrate stored in the dark is
903 represented by an arrow pointing from the dark phase to the light phase. Malate
904 storage is not illustrated in this diagram.
905
906 **Figure 7.** Comparison of model predictions between C_3 and the various subtypes of
907 CAM defined in Table II. The model predictions for photon use, Rubisco carboxylase
908 flux, Rubisco oxygenase flux, total flux through Rubisco and the total flux in the
909 metabolic model are shown with values scaled as a percentage of the value in the
910 C_3 leaf model.
911

Table I. *List of reactions in the light that have different fluxes in the diel model and the continuous light model*

Reactions with similarity measures less than 0.25 are listed, where a small value represents a large difference in fluxes from the two modelling approaches (see Supplemental Table II for a complete list of reactions with non-overlapping flux ranges). The metabolic context of the reactions is listed in the column on the right.

Reaction name	Similarity Measure	Metabolic context
Reactions with higher flux in the diel model		
Plastidic ADPglucose pyrophosphorylase	0	Starch synthesis
Plastidic starch synthase	0	Starch synthesis
Plastidic phosphoglucose isomerase	0	Starch synthesis
Plastidic phosphoglucomutase	0	Starch synthesis
Tonoplast citrate/H+ antiporter	0	Storage in the vacuole
Tonoplast malate/H+ antiporter	0	Storage in the vacuole
Tonoplast fumarate/H+ antiporter	0	Storage in the vacuole
Tonoplast nitrate transporter	0	Storage in the vacuole
Tonoplast PP_iase	0	Storage in the vacuole
Plastidic alkaline pyrophosphatase	0.015	Related to starch synthesis
Reactions with higher flux in the continuous-light model		
Peroxisomal inorganic pyrophophatase	0	Related to Glu and Gln synthesis
Peroxisomal phosphate transporter	0	Related to Glu and Gln synthesis
Peroxisomal citrate synthase	0	Related to Glu and Gln synthesis
Peroxisomal acetyl-CoA synthetase	0	Related to Glu and Gln synthesis
Peroxisomal AMP/ATP antiporter	0	Related to Glu and Gln synthesis
Peroxisomal acetate transporter	0	Related to Glu and Gln synthesis
Peroxisomal citrate transporter	0	Related to Glu and Gln synthesis
Cytosolic threonine aldolase	0.019	Related to Glu and Gln synthesis
Cytosolic aldehyde dehydrogenase	0.019	Related to Glu and Gln synthesis
Plastidic ATP/ADP antiporter	0.093	Export of ATP from the chloroplast
Plastidic threonine transporter	0.123	Related to Glu and Gln synthesis
Plastidic threonine synthase	0.145	Related to Glu and Gln synthesis
Plastidic homoserine kinase	0.153	Related to Glu and Gln synthesis
Plastidic homoserine dehydrogenase	0.161	Related to Glu and Gln synthesis
Plastidic aspartate kinase	0.180	Related to Glu and Gln synthesis
Plastidic aspartate semialdehyde dehydrogenase	0.180	Related to Glu and Gln synthesis
Mitochondrial ATP/AMP antiporter	0.202	Related to Glu and Gln synthesis
Mitochondrial aldenylate kinase	0.202	Related to Glu and Gln synthesis
Plastidic aspartate transporter	0.208	Related to Glu and Gln synthesis

Table II. *Constraints applied for modelling leaf metabolism in C_3 and various subtypes of CAM*

Constraints for different modes of photosynthesis		C_3	CAM				
			generic	starch-PEPCK	starch-ME	sugars-PEPCK	sugars-ME
CO_2 exchange	CO_2 exchange in light	Free	0				
Photorespiration	Rubisco CO_2:O_2	3:1	Unconstrained in light, 3:1 in dark				
Transporter	chloroplast G6P-Pi	0	Free				

Metabolic reactions	PEPCK	Free	Free	Free	0	Free	0
	ME	Free	Free	0	Free	0	Free
	pyruvate, P_i dikinase	Free	Free	0	Free	0	Free
Storage compounds	Starch	Free	Free	Free	Free	0	0
	Soluble sugars	Free	Free	0	0	Free	Free

921

922

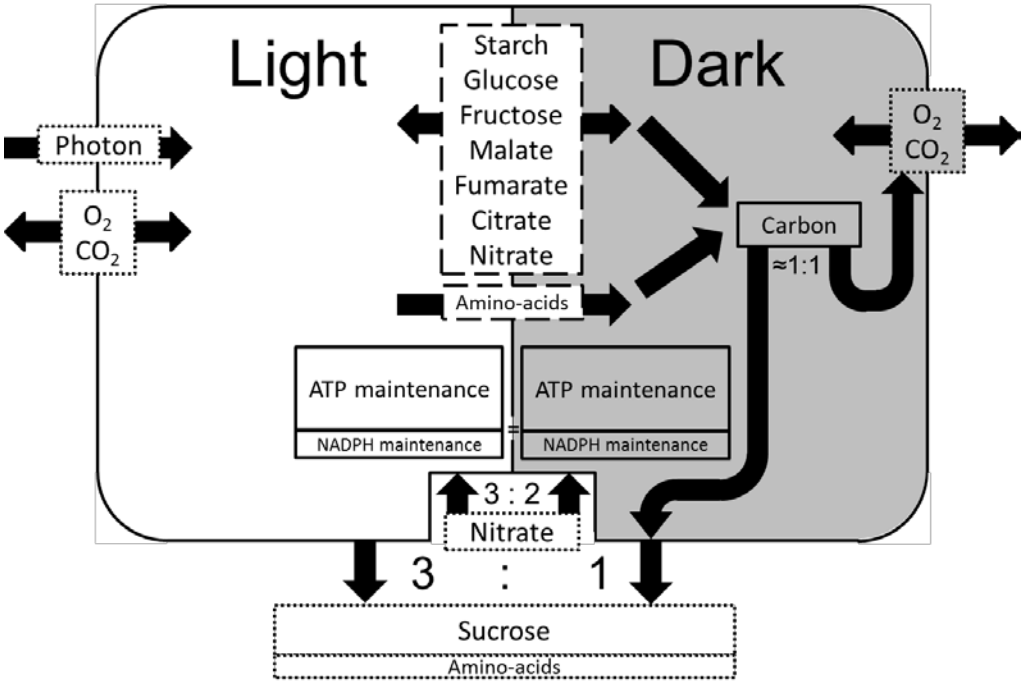

923

924

925 **Figure 1.** Flux-balance framework for integrated metabolic modelling of the day and
926 night phases of a mature leaf. The light dark phases are represented by the white
927 and grey backgrounds of the diagram respectively. Metabolites shown in the dashed
928 rectangles between the two phases represent potential storage compounds. Starch,
929 glucose, fructose, malate, fumarate, citrate and nitrate were allowed to accumulate in
930 the light and in the dark as denoted by the arrows pointing towards the light and dark
931 states. Twenty common amino-acids were allowed to accumulate in the light but not
932 in the dark as denoted by the arrow pointing from the light phase to the dark phase.
933 Export to the phloem was set to four sucrose to one amino-acid, with 18 different
934 amino-acids in the proportions shown in Supplemental Table 1.The export rate was
935 set to be three times greater in the light that in the dark. Nitrate was set as the sole
936 nitrogen source with the ratio of nitrate uptake from the phloem in the light to that in
937 the dark set to 3 to 2. Cellular maintenance costs in the dark were set to a fixed
938 value where the carbon exported during the night roughly equalled the carbon
939 released as CO_2 in the dark phase. Maintenance costs were assumed to be the
940 same in the light and the dark. The ratio of ATP maintenance cost to NADPH
941 maintenance cost was set to 3 to 1.

942

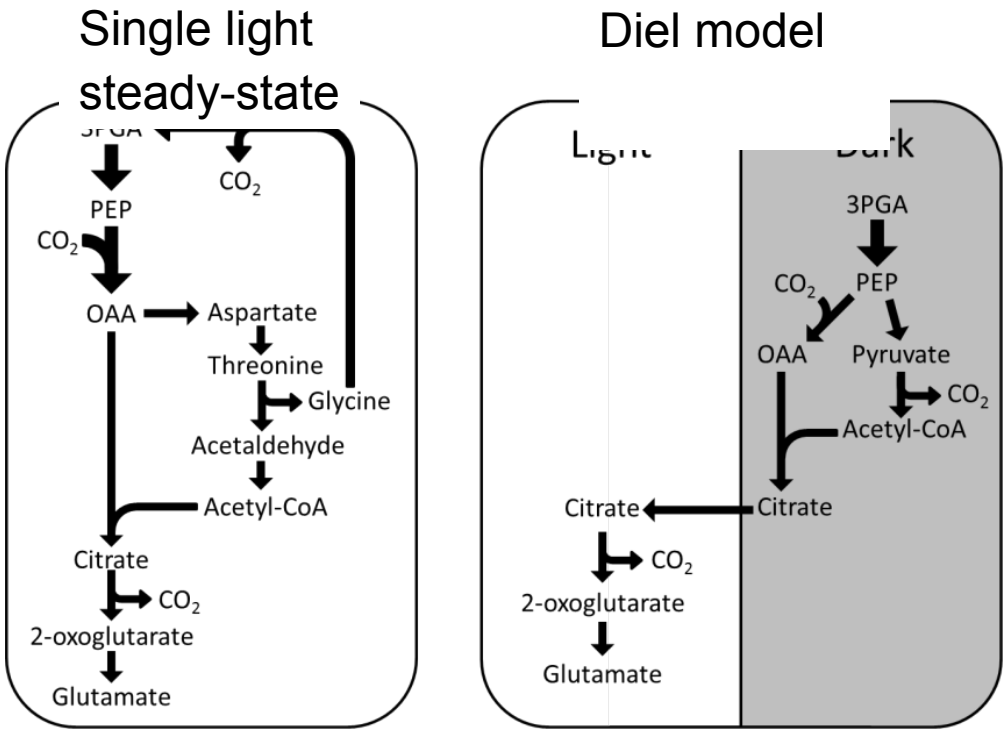

Figure 2. Metabolic routes for glutamate biosynthesis from two modelling approaches. A single steady-state model in constant light is shown on the left and the diel modelling framework on the right. In constant light, the carbon skeletons for glutamine synthesis were predicted to be supplied via a metabolic route in which threonine is metabolised in the cytosol to acetate, transported to the peroxisome and metabolised to citrate which is exported to the cytosol and converted to 2-oxoglutarate. Using the diel modelling framework, the model predicted the use of citrate stored in the dark to provide the carbon skeletons for glutamate synthesis in the light. Abbreviations: PEP, phospho*enol*pyruvate; OAA oxaloacetate. The thickness of the arrows is scaled to indicate relative flux magnitudes (in molar units).

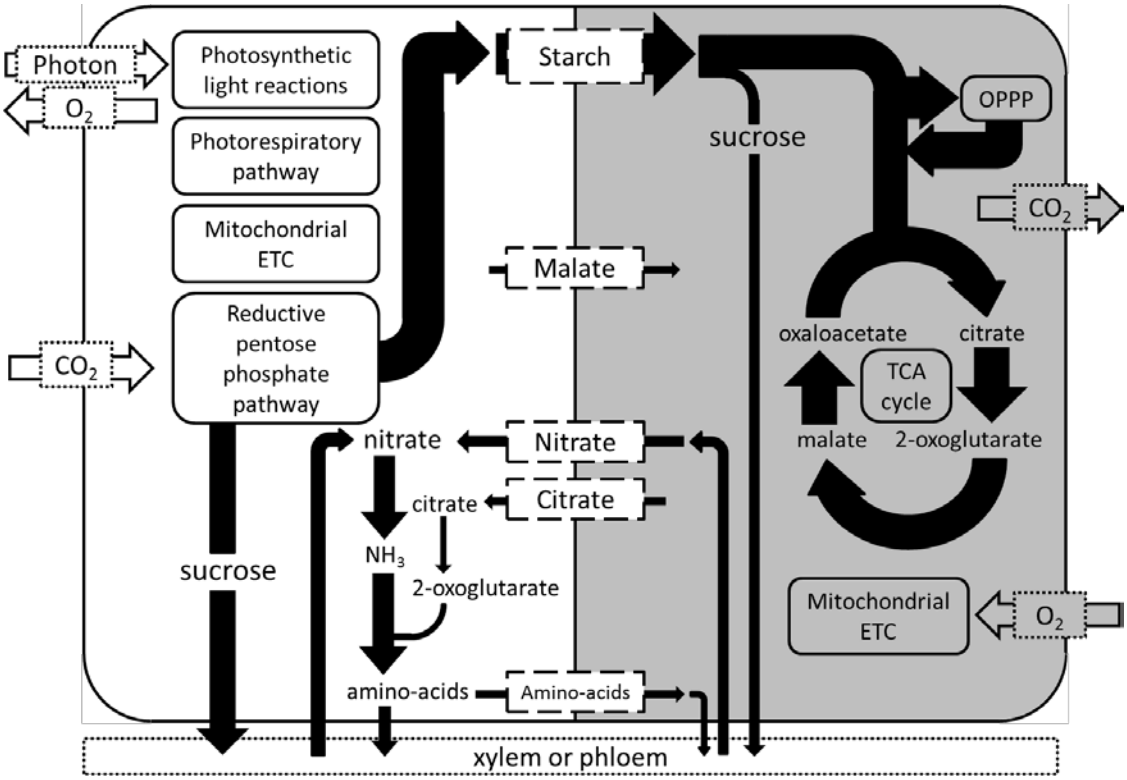

957

958

959

960 **Figure 3.** Predicted flux map of metabolism for a mature C_3 leaf over a day-night
961 cycle. The light dark phases are represented by the white grey backgrounds
962 respectively. Metabolites shown in the dashed rectangles between the two phases
963 represent storage compounds. The thickness of the arrows is proportional to the
964 metabolic flux through the reactions (in molar units). Metabolic processes listed
965 within rounded rectangles carry fluxes too large to be represented on the flux map.
966 Abbreviations: ETC, electron transport chain; OPPP, oxidative pentose phosphate
967 pathway; TCA, tricarboxylic acid.

968

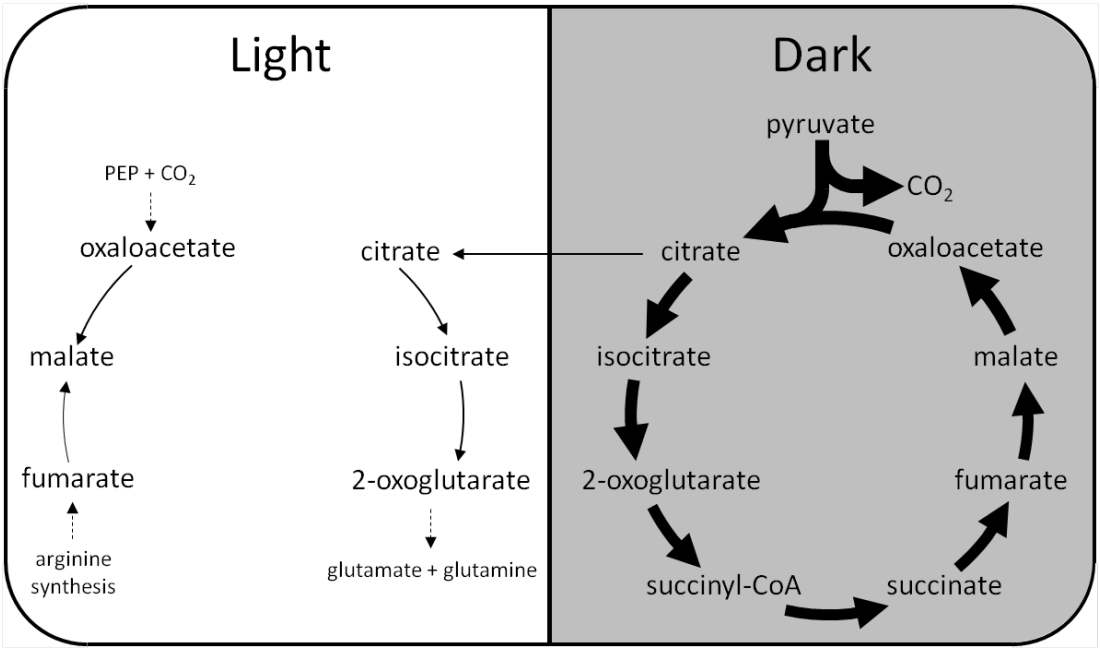

Figure 4. Flux predictions through the TCA cycle and pyruvate dehydrogenase in a C_3 leaf in the light and the dark. A non-cyclic mode with two separate branches, citrate to 2-oxoglutarate and oxaloacetate and fumarate to malate, was predicted to operate in the light. A cyclic mode of the TCA cycle was predicted to operate in the dark, mainly to produce ATP via oxidative phosphorylation. Fluxes illustrated are net conversion between metabolites over all subcellular compartments. The thickness of the arrows is proportional to the metabolic fluxes through the reactions (in molar units). Citrate stored in the dark is represented by an arrow pointing from the dark phase to the light phase. Malate storage is not illustrated in this diagram.

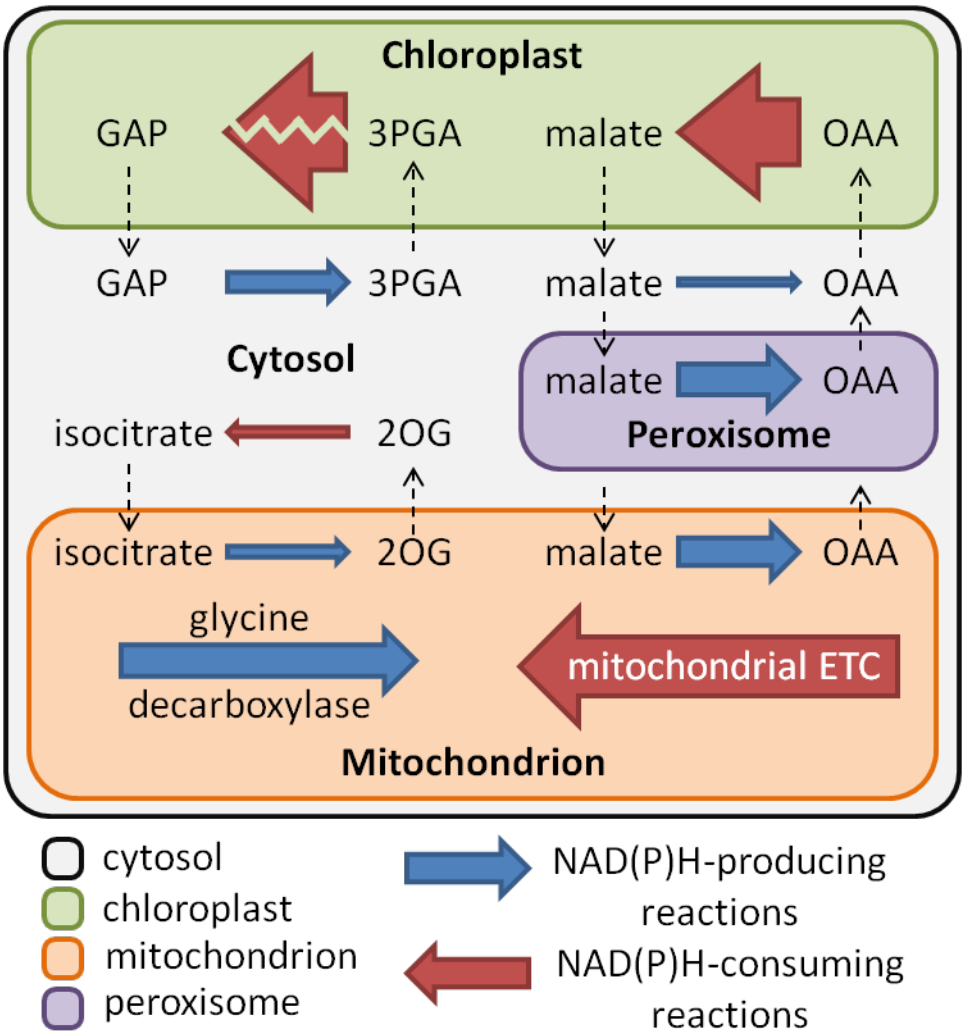

Figure 5. Reductant shuttling between subcellular compartments and the production and consumption of NADH in mitochondria in the light. Left-pointing arrows represent reductant-consuming reactions; right-pointing arrows represent reductant-producing reactions. The thickness of the solid arrows is proportional to the metabolic flux through the reactions (in molar units), except for the conversion between 3PGA and GAP in the chloroplast where the zig-zag line across the arrow indicates that the flux is too large to be illustrated to scale in the diagram. Reductant shuttles between four subcellular compartments, cytosol, chloroplast, mitochondria and peroxisome, are shown with dashed arrows representing transfer of metabolites between compartments. Abbreviations: 2OG, 2-oxoglutarate; 3PGA, 3-phosphoglycerate; ETC, electron transport chain; GAP, glyceraldehyde 3-phosphate; OAA, oxaloacetate.

997

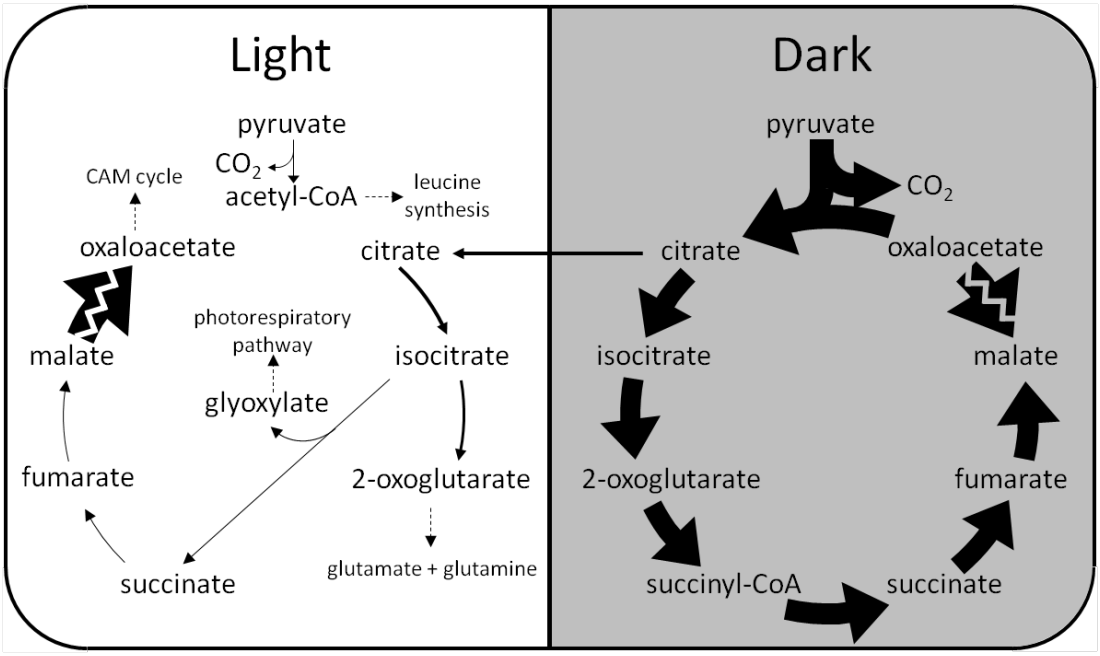

Figure 6. Flux predictions through the TCA cycle and related reactions in a CAM leaf. A non-cyclic mode with two distinct branches, citrate to 2-oxoglutarate and succinate to oxaloacetate, was predicted to operate in the light. The two branches of the TCA cycle are connected by isocitrate lyase which converts isocitrate into succinate and glyoxylate. A cyclic mode of the TCA cycle was predicted to operate in the dark, mainly to contribute to ATP production via oxidative phosphorylation. Fluxes illustrated are net conversion between metabolites over all subcellular compartments. The thickness of the arrows is proportional to the metabolic flux through the reactions (in molar units), except for the conversion between malate and oxaloacetate where the zig-zag line across the arrow indicates that the flux is too large to be illustrated to scale in the diagram. Citrate stored in the dark is represented by an arrow pointing from the dark phase to the light phase. Malate storage is not illustrated in this diagram.

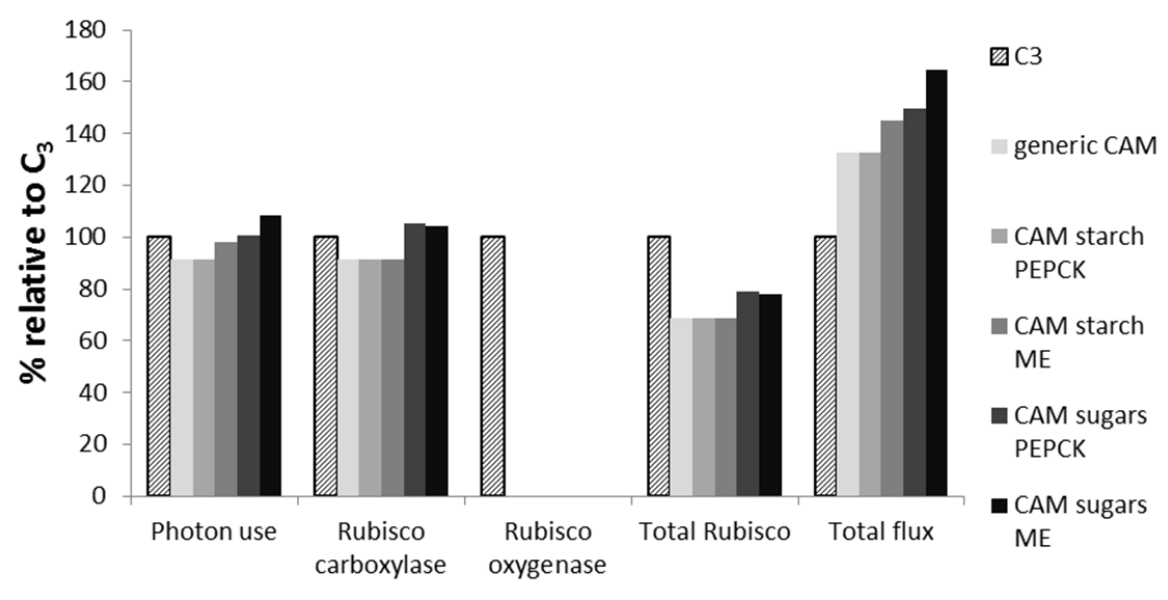

Figure 7. Comparison of model predictions between C_3 and the various subtypes of CAM defined in Table II. The model predictions for photon use, Rubisco carboxylase flux, Rubisco oxygenase flux, total flux through Rubisco and the total flux in the metabolic model are shown with values scaled as a percentage of the value in the C_3 leaf model.